A Mechanical Model for Collagen Fibril Load Sharing in Peripheral Nerve of Diabetic and Nondiabetic Rats

B. E. Layton
Department of Biomedical Engineering,
The University of Michigan,
Ann Arbor, MI 48109-2125

A. M. Sastry*
Fellow, ASME
Department of Mechanical Engineering,
and Department of Biomedical Engineering,
The University of Michigan,
Ann Arbor, MI 48109-2125

Peripheral neuropathy affects approximately 50% of the 15 million Americans with diabetes. It has been suggested that mechanical effects related to collagen glycation are related to the permanence of neuropathy. In the present paper, we develop a model for load transfer in a whole nerve, using a simple pressure vessel approximation, in order to assess the significant of stiffening of the collagenous nerve sheath on endoneurial fluid pressure. We also develop a fibril-scale mechanics model for the nerve, to model the straightening of wavy fibrils, producing the toe region observed in nerve tissue, and also to interrogate the effects of interfibrillar crosslinks on the overall properties of the tissue. Such collagen crosslinking has been implicated in complications in diabetic tissues. Our fibril-scale model uses a two-parameter Weibull model for fibril strength, in combination with statistical parameters describing fibril modulus, angle, wave-amplitude, and volume fraction to capture both toe region and failure region behavior of whole rat sciatic nerve. The extrema of equal and local load-sharing assumptions are used to map potential differences in diabetic and nondiabetic tissues. This work may ultimately be useful in differentiating between the responses of normal and heavily crosslinked tissue.
[DOI: 10.1115/1.1824118]

Introduction

Alterations in fibrillar collagens have been implicated in a wide variety of progressive disorders, including osteogenesis imperfecta, chondrodysplasias and osteoarthritis [1–3]. Cardiovascular disease [4], and diabetic polyneuropathies [5–7] have also been linked to alterations in fibrillar collagens. The latter disorder is the leading cause of morbidity associated with diabetes [8], and is related to complications in injuries that often result in amputation [9,10].

The etiopathology of this disease likely involves the remodeling of extracellular matrix (ECM) proteins such as collagen [11]. In diabetic neuropathy, fibrillar collagens become glycated [12], resulting in larger [5–7] and possibly more highly crosslinked [13] fibrils. Because of the importance of fibrillar collagens in preserving signal fidelity and offering mechanical protection [14,15] in peripheral nerve tissue, their alteration due to glycation has been the subject of intense study in recent years, spanning biochemical assays of advanced glycation end-product formation [16], fibril diameter alterations [5–7] and degree of advanced glycation end product (AGE) and other types of crosslinking [17]. Indeed, a leading hypothesis regarding damage in peripheral neuropathy holds that crosslinking due to excessive glycation of peripheral nerve tissue of AGEs impairs the regrowth of axons, and thus impairs electrical signal transduction in the nerve [5].

Collagen fibrils encase the peripheral nerve (Fig. 1), and ensheath the conductive axons, which follow wavy courses through the endoneurium; the endoneurium is surrounded by the perineurium, a multi-cellular layer of tight-junction-connected flattened cells. The densely collagenous, relatively acellular epineurium surrounds the perineurium (Fig. 2) [18–24]. Work on modeling tissue ''stiffening'' has also increased dramatically in recent years, due to its importance in a host of diabetic complications such as foot ulcerations [25,26], and several approaches have been developed to model the mechanical behavior of fibrillar collagen-reinforced tissues such as skin [27,28]. Continuum approaches have proven to be excellent tools for modeling soft tissue response [29,30], and have allowed a characterization of collagenous tissues such as ligament [31]. However, the connections between the physical properties of the microscale components of collagenous tissue, and the tissue itself (Fig. 3) remain to be determined in many important clinical applications, including tissue stiffening due to collagen glycation.

Our objective in the present work is to use our own and other clinical data [7,32] to build micromechanical models for deformation of the fibrillar collagens of peripheral nerve. We seek a way of correlating generalized tissue ''stiffening'' reported throughout the literature, with molecular and fibril-scale data we have obtained on healthy and diabetic tissues. Both greater densities of collagen fibrils and greater densities of glycation-induced crosslinks among them, would generally be expected to result in (1) the upregulation of collagen via increased localized stress on collagen producing cells (e.g. fibroblasts or perineurial cells), (2) resultant stiffening of the collagenous sheath of the nerve trunk, and finally, (3) increased endoneurial fluid pressure (EFP). Positive feedback among these effects may be clinically significant; observed increases in diabetic EFP [33,34], for example, may be sufficient to cause permanent nerve dysfunction. A full understanding of the combined biochemical/mechanical origins of EFP increases may provide a therapeutic target. Also, the quantitative linkage of increases in the fibril diameter in diabetic collagens due to glycation may offer an independent and relatively benign clinical assay of collagen glycation, since a very small amount of tissue, obtainable via a simple needle punch, is sufficient to survey fibril diameters using atomic force microscopy (AFM) [7].

Arrangement and Composition of Epineurial Fibrillar Collagens. Of the three fibrillar collagens (I,III,V) found in a peripheral nerve, type I collagen is most abundant, appearing in a

*Correspondence to Professor Ann Marie Sastry, Department of Mechanical Engineering, 2140 GGBrown, 2350 Hayward St., Ann Arbor, MI 48109-2125. E-mail: amsastry@engin.umich.edu; fax: (734) 647-3170; telephone: (734) 764-3061.

Contributed by the Bioengineering Division for publication in the JOURNAL OF BIOMECHANICAL ENGINEERING. Manuscript received by the Bioengineering Division August 1, 2003; revision received April 27, 2004. Associate Editor: Louis Soslowsky.

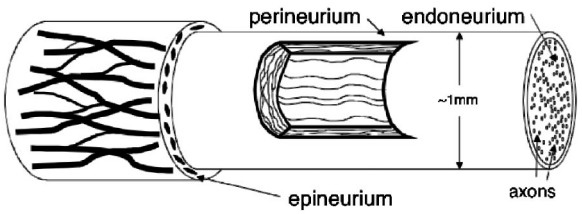

Fig. 1 Rat sciatic nerve anatomy, including endoneurium, perineurium, and epineurium. This single-fascicled nerve is often used as a model for a human peripheral nerve, which typically has several perineuria within a single epineurium.

4:1 ratio with type III [35]; much work, summarized in Table 1 (per [36–41]), has been done to isolate and quantify these collagens. Type V is also present, but to a lesser extent than types I and III [5,42]. Afibrillar collagens are also present in the peripheral nerve, with type IV present in the basement membranes of cells such as axons, Schwann cells, perineurial cells, and blood vessels [43], and type VI present in networks among Schwann cells and blood vessels in neurofibromas [44] and are also likely involved in local load transfer to cells. It is the fibrillar bundle-forming collagens such as types I and III that are responsible for the nerve's axial mechanical behavior.

Epineurial collagen fibrils are arranged in wavy bundles [46] with widths on the order of 10–20 μm [46]. Bundles found among the perineurial cells are smaller, on the order of 3 μm (containing ~1000 fibrils), and self-assemble into a ''lacework'' structure [46]. These bundles are only visible via scanning electron microscopy (SEM) after cellular digestion. Imaging of the inner surface of a stripped perineurium with atomic force microscopy (AFM) often reveals no collagens [7], implying that the inner surface of the perineurial cells is relatively smooth and continuous, and not tightly connected to the endoneurium.

High resolution imaging modes such as AFM, SEM, and TEM (transmission electron microscopy) are not capable of distinguishing among fibrillar collagen types such as types I, III, and V, since all display 64 nm periodicity. Collagen type must be determined with techniques such as immunofluorescent tagging (Table 1). In a rat sciatic nerve, the epineurium and perineurium are tightly connected [45], and thus, we hereafter use the epineurium/perineurium to denote the combined layers.

From our work using AFM [7], and from earlier results from scanning electron microscopy (e.g., [46]) collagen fibrils are longer than the gage lengths of most mechanical test specimens. For example, images of two [46] or three [7] orders of magnitude smaller than a typical test specimen (10 mm), fibril ends are not seen. Ends have been observed only in samples prepared *in vitro* [47] or in embryonic tissues [48]. Other workers have conjectured that collagenous tissue is comprised of fibrils simply of ''indefinite length'' [49]. A linear extrapolation from the growth curves of Birk et al. [48], perhaps the most exhaustive study of *in vivo* fibril length found the growth rate of collagen fibrils of embryonic chick tendon to be 6.5 μm/day, and while a linear extrapolation of this growth rate results in average fibril lengths of only ~1 mm in a typical tissue sample as might be taken from a 3-month-old rat, fibril–fibril aggregation is also possible.

Glycation and Structural Changes. A complete understanding of the structural effects of excessive glycation on structural collagens (e.g. interfibrillar crosslinking, alterations in axial properties, etc.) has not yet been achieved, though increased expression has been found in glycated fibrillar and afibrillar collagens, *in vitro* [50]. Increased collagen fibril diameters (Fig. 4) have also been found in fibrillar collagens in diabetic tissues [5–7], resulting from glycation [51]. Larger fibrillar diameters in collagens have also been positively correlated with the increasing severity of diabetic neuropathy [5].

Structural alterations in collagens glycated *in vitro* have also been observed. Deeper clefts in D-bands of diabetic rat tail collagen fibrils have been attributed to increased crosslink density [51]. This hypothesis is supported by x-ray crystallographic data of *in vitro*-glycated collagen [52], but may be part of the natural growth pattern of collagen [53]. Crosslinking among collagen

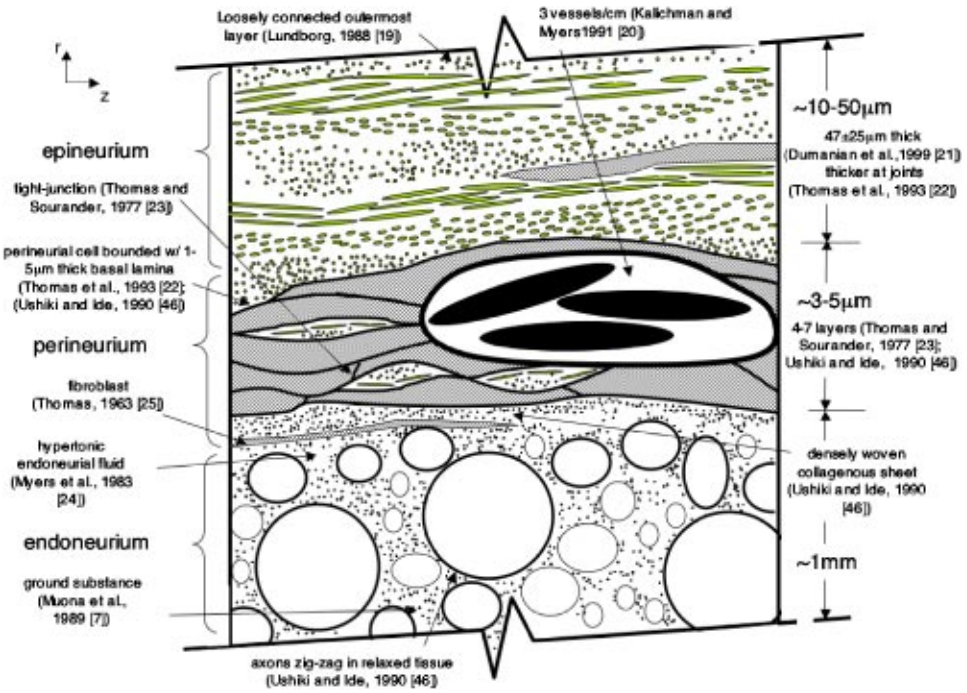

Fig. 2 Transperineurial view of peripheral nerve, showing relative locations of cells, and extracellular matrix. Elliptical sections in the epineurium are oblique sections through collagen fibrils.

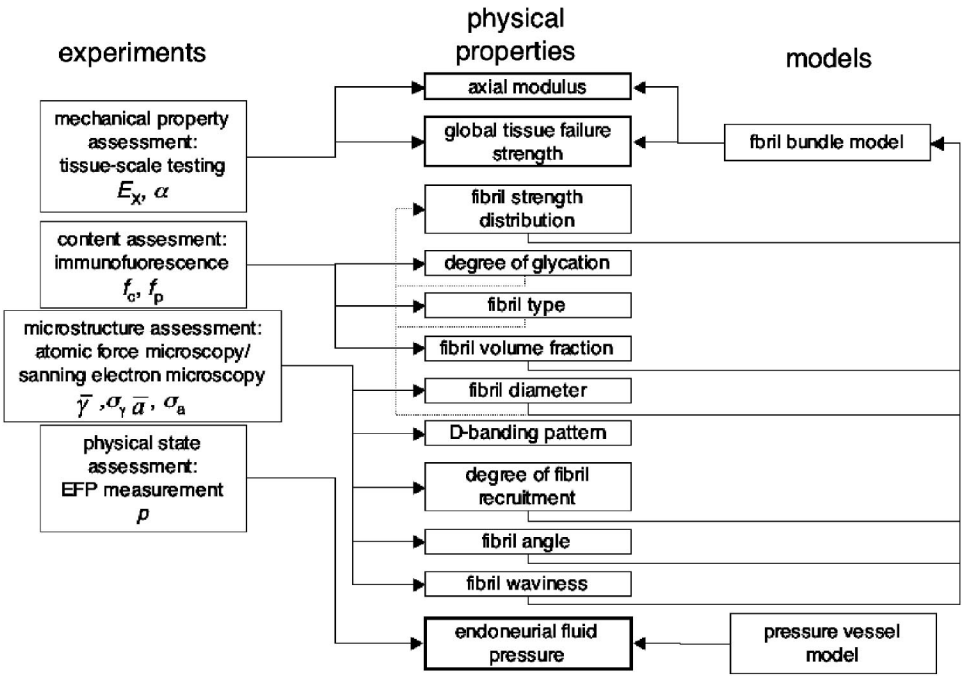

Fig. 3 Experiments, and models designed to determine and understand the role of mechanical properties of the peripheral nerve in the permanence of diabetic neuropathy. Bold boxes denote physical properties strongly associated with both experiments and models. Dashed lines denote the possible relationships not investigated in the present model, but likely to affect the properties studied.

fibrils due to the formation of advanced glycation end-products (AGEs) has been implicated in the stiffening of collagenous tissue such as skin [27,28]. Such crosslinking has been associated with oxidative stresses [54], which are among many adverse outcomes of poor metabolic glucose control [55].

Load Transfer in Fibrillar Collagens. A number of models have been developed to describe the viscoelastic properties of a healthy [56] and surgically repaired [57,58] peripheral nerve using continuum mechanics-based approaches. These materials exhibit classic bundle-type stress-strain behavior: straightening of fibers produces an initial ''toe region,'' followed by a linear response (Fig. 5). Recently, micromechanical approaches have also been proposed, including work by Roeder et al. [59], building on a model by Parry [60], in which stress–strain curves from the toe region to failure were constructed using 3-D structural properties of reconstituted, low-volume fraction collagens. Hurschler et al. [61] used a combined macro-microscale, seven-parameter model to capture the gross mechanical properties of the tendon. More recently, geometry-based models have been developed to characterize the toe region, from variables such as the average fibril

Table 1 Collagen types and locations in peripheral nerve and a summary of methods used for their detection. DRG=dorsal root ganglion, en=endoneurium, ep=epineurium, fem=femoral, fib=fibrosis, IHC=immunohistochemistry, ISH=in situ hybridization, pe=perineurium, n.=none, n.d.=not done, REV=review article, sc=sciatic, su=sural.

Year	Author	Animal	Nerve	Method	I	II	III	IV	V	VI	Laminin	Fibronectin	Concentration
2001	Podratz et al. [37]	rat	DRG	IHC	n.d.	n.d.	n.d.	n.d.	n.d.	n.d.	en	n.d.	n.a.
2000	Williams et al. [38]	human	su	IHC	n.d.	n.d.	n.d.	en, pe	n.d.	n.d.	n.d.	n.d.	no change in diabetics
2000	Bradley et al. [6]	human	su	IHC	en, pe, ep	n.	en, pe, ep	en, pe	en, pe	pe, ep	en, pe	en, pe, ep	increased in diabetics
1997	Lowry et al. [39]	human	sc, su	IHC	n.d.	n.d.	n.d.	en, pe	n.d.	n.d.	n.d.	n.d.	related to fascicle perimeter
1992	Lorimer et al. [44]	rat	sc	IHC	en, ep, pe	n.d.	ep, pe, en	ep, pe, en	n.d.	n.d.	en, ep, pe	en, ep, pe	low type I in peri
1990	Peltonen et al. [40]	human	n.g.	ISH, IHC	whole	n.d.	whole	n.d.	n.d.	whole	n.d.	n.d.	increased in neurofibroma
1986	Fujii et al. [92]	human	tibial	PAGE	whole	n.d.	whole	n.d.	n.d.	n.d.	n.d.	n.d.	16% dry weight
1985	Fleischmajer et al. [45]	human	n.g.	IHC	fib	n.d.	fib	fib	fib	fib	fib	n.d.	increased in neurofibroma
1985	Salonen et al. [43]	rat	sc	IHC	en, ep	n.d.	en, pe, ep	n.d.	en, pe	n.d.	n.d.	en	increased post transection
1984	Carbonetto [41]	REV	REV	REV	en	n.	en	en	en	n.g.	en	en	REV
1979	Shellswell et al. [42]	bovine	sc	PAGE	whole	n.d.	whole	en, pe	en, pe	n.d.	n.d.	n.d.	more III in endo and peri than epi
1977	Seyer et al. [36]	human	fem	cellulose	whole	n.d.	whole	n.d.	n.d.	n.d.	n.d.	n.d.	I:III=4:1

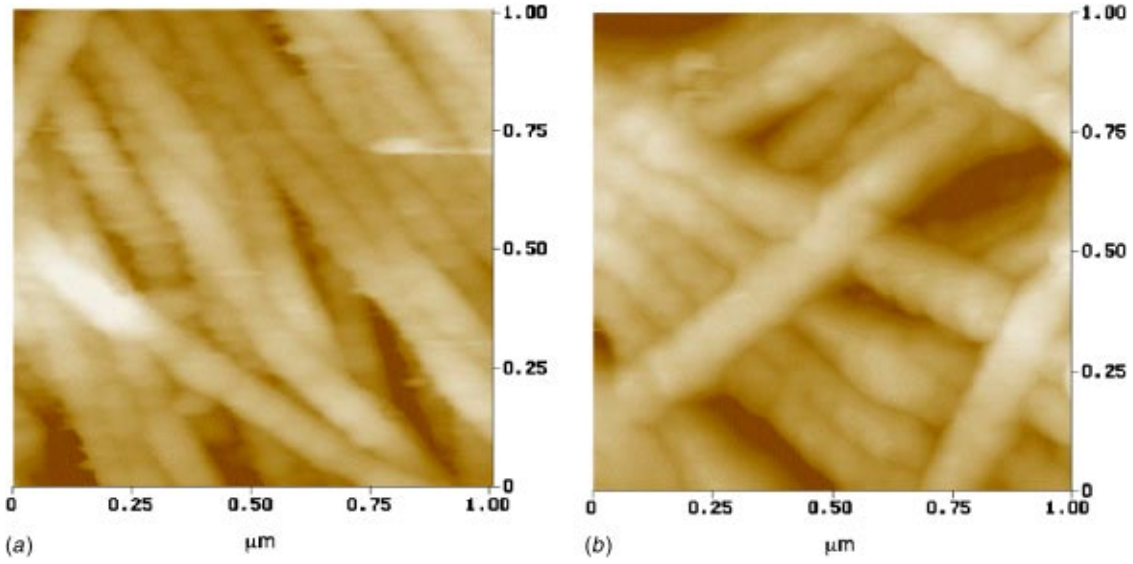

Fig. 4 Comparative images of fibrillar epineurial collagens of healthy and diabetic peripheral nerve [7] revealing larger fibril diameters in the diabetic tissue

angle [62]. These microscale approaches have shown promise in determining contributions from various elements of tissue to resistance to mechanical stress. Other work has focused on the role of stress-induced collagen upregulation by cells such as fibroblasts (e.g. [63]) or increased glucose concentrations [64].

Additionally, the possible physical connections (i.e. chemical crosslinks) resulting from excessive glycation among (e.g. [65,66]) or within (e.g. [52,67]) the roughly collimated collagen fibrils may alter their load sharing when deformed axially. Though we have previously measured the stress–strain response [32] at high, nonphysiological loads [14,15], such data can allow inference as to the construction of the material. Spatial arrangement, mechanical stiffness, mechanical strength, content, and fibril diameter distributions [5–7] of extracellular matrix proteins [68] such as collagen affect the structural mechanics of the peripheral nerve at both the microscale and tissue scale. Importantly, the inherent waviness in the fibrillar collagens of the peripheral nerve produces inherently nonlinear behavior, though the fibrils themselves are well-modeled as elastic elements, as we show. Sequential failure in the fibril bundles produces additional nonlinear behavior, even though the fibrils are assumed elastic. Thus, high strain behavior is modeled even as the fibrils are assumed to align, then subsequently rupture, at realistic, low strains.

Ultimately, our goal is to use this model to determine the effect of altered composition of peripheral nerve collagens, especially interfibrillar crosslinking, on mechanical properties. Our implicit hypothesis in developing this model is that diabetic tissues exhibit more local load-sharing, due to crosslinking of collagens by glycation. This hypothesis, however, is not directly tested here. Rather, this work demonstrates the ability of the model to characterize the collagen-rich tissue of the rat sciatic nerve. Future work will be dedicated to quantifying differences in diabetic and healthy tissues using the model. Such comparisons may be useful in diagnosing and treating disorders and injuries such as compression neuropathies [69,70], diabetic neuropathies [71], hereditary motor and sensory neuropathy [5] and neural fibromas [72], via a determination of the state of crosslinking in collagenous tissues.

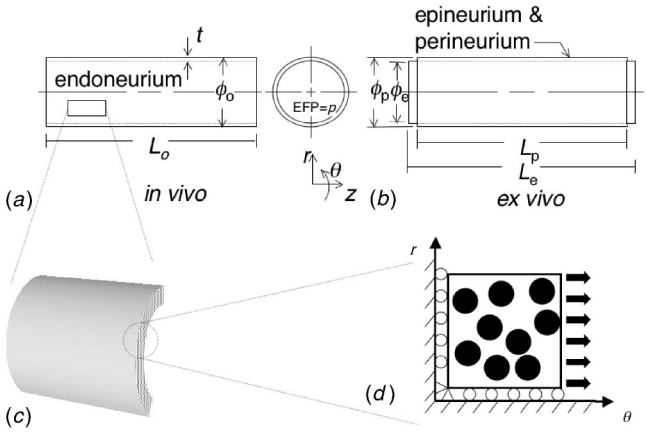

Fig. 5 Pressure vessel model of single-fascicled rat sciatic peripheral nerve in its (*a*) in vivo, and (*b*) ex vivo states. Upon excision, the perineurium and epineurium retract, effectively extruding the endoneurium. Loads in the epineurium/perineurium of a peripheral nerve, showing (*c*) a "continuum" section, and (*d*) the depiction of how in-plane fibril distributions affect load sharing among the fibrillar collagens.

Methods: Theory

We develop models for nerve tissue response at two scales: first, for whole nerve, we derive a simple pressure-vessel model to estimate internal pressure, and its relationship to axial and transverse stiffening. Second, for axial response of the collagenous epineurium/perineurium, we develop a fiber bundle model, to capture the toe (straightening of fibrils), linear (stretching of fibrils) and yield (sequential failure of fibrils, dependent upon fibril crosslinking) regions of the stress–strain curve.

Structural Model of the Peripheral Nerve: Internal Pressure and Stiffening. We model the nerve as a layered, cylindrical, linear elastic pressure vessel (Figs. 5(*a*), 5(*b*)). For the combined epineurium/perineurium, assuming anisotropic plane strain, we write

$$\varepsilon_{\theta\theta} = \frac{\sigma_{\theta\theta}}{E_{\theta\theta}} - \nu_{z\theta}\frac{\sigma_{zz}}{E_{zz}}, \tag{1}$$

$$\varepsilon_{zz} = -\nu_{\theta z}\frac{\sigma_{\theta\theta}}{E_{\theta\theta}} + \frac{\sigma_{zz}}{E_{zz}}, \tag{2}$$

and

Table 2 Parameters used/obtained in simulations and experiments

Parameter	Value	Description	Origin
$\overline{E_f}$	0.1–0.5 GPa	Average fibril modulus	Estimated from whole nerve uniaxial data in current work
f_c	0.1	Area fraction of collagenous portion of whole nerve	Estimated from Seyer et al. 1977 [35]
f_p	0.7	Area packing fraction of collagen within collagenous portion of nerve	Estimated from Muona et al. 1989 [6]
$\overline{\gamma}$	0	Average fibril angle in radians (zero for all simulations)	Calculated from model and compared to Ushiki and Ide [46]
σ_γ	0–0.82	Standard deviation of fibril angle in radians (0=parallel to nerve axis)	Calculated from model and compared to Ushiki and Ide [46]
$\overline{a}$	0–1	Fibril amplitude normalized to fibril sinusoidal spatial wavelength	Calculated from model and compared to Ushiki and Ide [46]
σ_a	0–0.35	Standard deviation of fibril amplitude	Calculated from model and compared to Ushiki and Ide [46]
E_x	0–1	Normalized fibril Weibull scale parameter strength/modulus	Calculated from model
α	0–10	Fibril Weibull shape parameter	Calculated from model

$$\nu_{\theta z}=\nu_{z\theta}\frac{E_{\theta\theta}}{E_{zz}}. \tag{3}$$

where ε is strain, σ is stress, E is the elastic modulus, and ν is Poisson's ratio. Subscripts $\theta\theta$ and zz denote tangential and axial directions, respectively. Force equilibrium in the hoop direction, between the inner (endoneurium) and outer (epineurium/perineurium) concentric layers, requires that

$$\sigma_{\theta\theta}=\frac{p\phi_0}{2t}, \tag{4}$$

and

$$\sigma_{zz}=\frac{p\phi_0}{4t}, \tag{5}$$

where p is the endoneurial fluid pressure, ϕ_0 is the *in vivo* endoneurial diameter, and t is the epineurial/perineurial thickness. We have the strain definitions

$$\varepsilon_{zz}=\frac{L_p-L_0}{L_0} \tag{6}$$

and

$$\varepsilon_{\theta\theta}=\frac{\phi_p-\phi_0}{\phi_0}. \tag{7}$$

For convenience, we define dimensionless parameters $\xi=E_{\theta\theta}/E_{zz}$, $\eta=t/\phi_e$, $\lambda=L_p/L_0$, and $\beta=\phi_p/\phi_0$, where L_0 and L_p are *in vivo* and *ex vivo* epineurial/perineurial lengths, respectively, and ϕ_p is the *ex vivo* epineurial/perineurial diameter. An expression for the endoneurial fluid pressure, p, based on five parameters obtainable via excision and measurement of a nerve, and a tensile mechanical test of the nerve trunk, can thus be written as

$$p=\left\lfloor\frac{4\xi\eta(\lambda+1-2\beta)}{\xi-4}\right\rfloor E_{zz}. \tag{8}$$

Several authors have previously estimated the tangential modulus of a peripheral nerve (e.g., [34,73–75]). Their reported values for Young's moduli of peripheral nerve tissues have ranged from 10 to 100 MPa [57,76]. We estimated a modulus using a dimensionless parameter, ξ, the ratio of hoop modulus, $E_{\theta\theta}$, to axial modulus, E_{zz}. We assumed that $\xi<1$, because of the preferential axial alignment of peripheral nerve collagen; this implies $\nu_{\theta z}<\nu_{z\theta}$ (Eq. (3)). The two parameters likely to have the strongest influence on this ratio, ξ, are (1) the average collagen fibril angle, and (2) the degree of interaction among fibrils due to either entanglement or interfibril crosslinks, or (3) the fraction of fibrils sharing triple helices.

Load-Sharing in Reinforced, Fibrillar Collagen Sheaths: Statistical Modeling. Our model stems from work by Harlow and Phoenix [77]. We simplified this model by approximating collagen fibrils as single, contiguous bundles, spanning typical 10 mm test specimen lengths [78]. This assumption is supported by our prior work in imaging peripheral nerve collagens [7] and from the growth curves of other collagenous tissues [48].

Seven independent variables, represented by nine model parameters, were required (summarized along with ranges in values used here, in Table 2): average fibril modulus, $\overline{E_f}$, collagenous area fraction of nerve, f_c, packing fraction of collagen, f_p, average, $\overline{\gamma}$, and standard deviation, σ_γ, of collagen fibril bundle angle, γ, average, $\overline{a}$, and standard deviation, σ_a, of collagen fibril amplitude, a, Weibull scale parameter, x_0, and Weibull shape parameter, α. Ideally, if $\overline{E_f}$, f_c, and f_p are known for a given tissue sample a priori, they can be used in the model as independent, specimen-specific variables. In this work, f_c was taken as 0.1 [35] and f_p as 0.7, [7]; $\overline{E_f}$ was taken directly from the linear portion of stress–strain curves found in our previous work [32].

To obtain fibril-bundle-scale morphology and confirm our estimations of collagen fibril and collagen fibril bundle morphology, images from Ushiki and Ide [46] were analyzed. Bounds for rat sciatic nerve EFP (0.2–1.0 kPa) were taken from the data of Myers et al. [33,79,80]. Reported failure strengths of collagen fibrils (2–70 MPa) [81,82] were reviewed to provide input to the model. Values for collagen fibril stiffness used were within those measured for reassembled fibrils (1–6 MPa) [83] and bovine Achilles tendon (430 MPa) [84]. The approximate density of collagen fibrils in peripheral nerve in the number of fibrils per square millimeter ($NF\cdot\mathrm{mm}^{-2}$) was estimated from

$$NF\cdot\mathrm{mm}^{-2}=\frac{4f_pf_c}{\pi d_f^2}. \tag{9}$$

Using approximate values of $f_p\approx0.7$, $f_c\approx0.1$, and $d_f\approx50$ nm, we estimate that there are $\sim3.5\times10^7$ fibrils/mm^2 in peripheral nerve tissue. To reduce the computational burden of generating thousands of simulations required for this each condition with a full set of fibrils, we chose to ''bin'' the fibrils into sets of eleven, in each simulation. An odd number of fibrils was chosen so that one fibril was aligned with the nerve axis; the use of fewer than eleven fibril groups resulted in solutions that were not capable of attaining smooth root-mean-squared (RMS) difference maps between

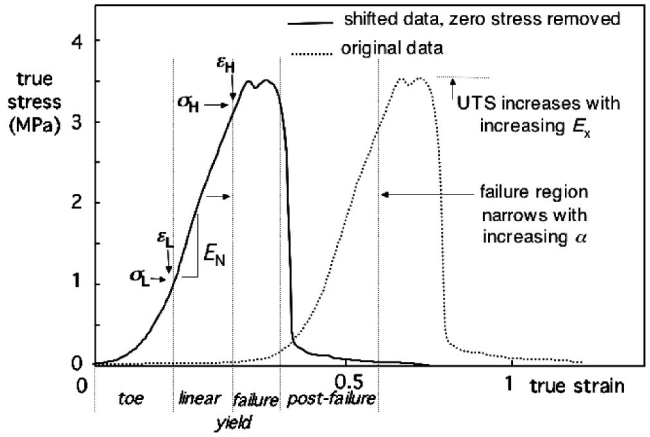

Fig. 6 A typical stress–strain response of fibrillar collagenous tissue of the peripheral nerve (data taken from failure curve of whole sciatic from a BioBreeding rat [32]) with toe, linear and failure regions noted. Notation for the bundle model is included.

experimental and simulated tissue. Simulations using greater than eleven fibril groups resulted in only minor improvements in smoothness, relative to the computational burden.

To model experimental uniaxial stress–strain curves from whole rat sciatic nerve (Fig. 6) using our simulated bundles, we first determined the effective fibril modulus via

$$\overline{E_f} = f_p f_c \frac{\sigma_H - \sigma_L}{\varepsilon_H - \varepsilon_L}, \tag{10}$$

where $\overline{E_f}$ is the average fibril modulus, ε_L and ε_H are the least and greatest strain values of the linear portion of a stress strain curve, and σ_L and σ_H are the least and greatest stresses of the linear portion of a stress strain curve. The ratio $([\sigma_h - \sigma_l]/[\varepsilon_h - \varepsilon_l])$ (Eq. (10)) is the whole nerve modulus, denoted E_N (Table 2). For the experimental curve used in this paper, a fibril modulus of 336 MPa was used. Using MATLAB-scripted software (Fig. 7(*a*)) batches of simulations were performed, generating stress–strain responses in the bundles to strain ε_H. The root-mean-squared (RMS) difference between experimental stress data points and linearly interpolated corresponding stress values of the simulated data was calculated for each case. Values for $\overline{a}$, σ_a, and $\sigma_\gamma(\overline{\gamma} = 0)$ were determined from these simulations, by minimizing RMS errors between simulated and experimental results. Typical experimental curves contained between 100 and 200 data points.

Simulations were run with approximately the same number of strain increments in each case, with simulations proceeding as follows. First, fibrils comprised of ten segments and having sinusoidal waviness (Fig. 7(*b*)) were generated. The fibril length, L', was determined from the curvilinear length, s, via

$$L' = \int_A^B \sqrt{1 - (s'(x))^2}\, dx. \tag{11}$$

Uniform data sets were used to generate normal distributions for averages $\overline{a}$, and standard deviations σ_a and σ_γ. These variables were then scaled linearly to map to a smooth domain. Normal

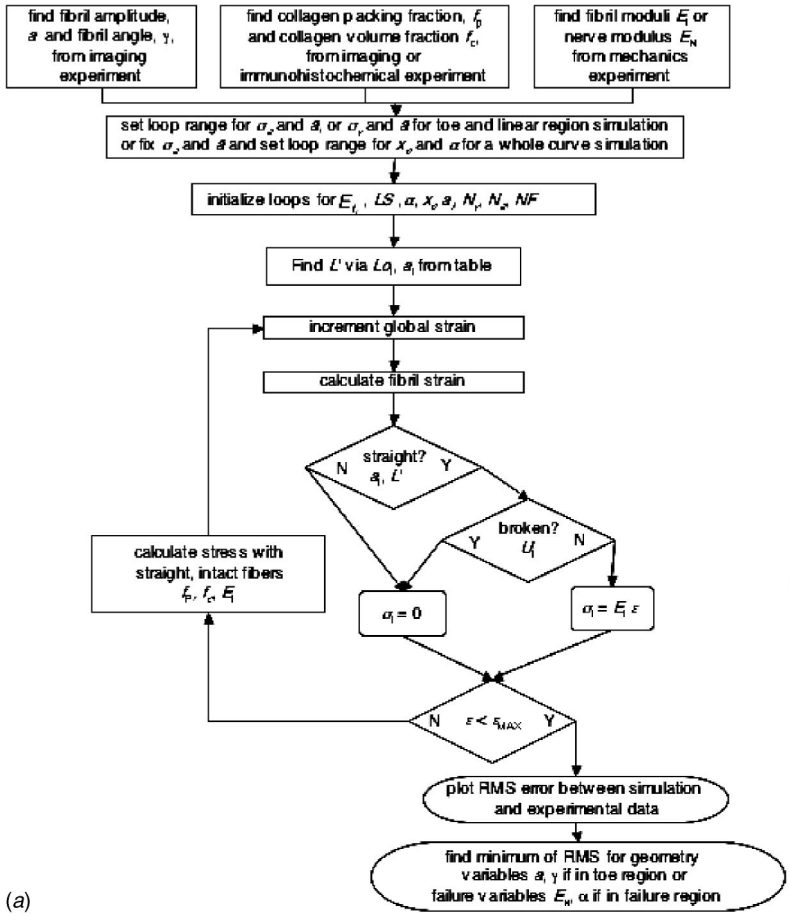

Fig. 7 Experimental data are fit with a series of simulations stepping through values for $\overline{a}$, σ_a, σ_γ, α and E_x with software depicted by (*a*) flow-chart for obtaining RMS minimum in bundle model, using (*b*) sinusoidal approximations of collagen fibrils

distributions were generated using the ANORM function from the Visual Numerics library [85]. Individual amplitudes, a_i, were assigned as normal distributions scaled and shifted by $\bar{a}$ per

$$a_i = \frac{N_a \Phi^{-1}(x_i)}{N_0} \bar{a} + \bar{a}, \tag{12}$$

where values of $N_a \in (0,0.05,0.1,\ldots,3.0)$ were chosen to scale the normally distributed amplitude data, $N_0 = \Phi^{-1}(1-\varepsilon)$, with $\varepsilon = 10^{-4}$, and

$$x_i = \left(\frac{1}{NF+1}, \frac{2}{NF+1} \cdots \frac{i}{NF+1} \cdots \frac{NF}{NF+1} \right). \tag{13}$$

Angles were similarly generated, per

$$\gamma_i = \frac{\pi}{2} \frac{N_\gamma \Phi^{-1}(x_i)}{N_0}, \tag{14}$$

where values of $N_\gamma \in (0,0.05,0.1,\ldots,3.0)$ were chosen to scale normally distributed angle data, and x_i were as in Eq. (13). For each simulation, as the global strain was incremented, fibrils were first checked for straightness, using Eq. (11). If straight, the force in the fibril was calculated using its modulus, and the strain along its axis. The axial component of this force was then added to the total force of the nerve. The total stress in the nerve was calculated as the total axial force of all straight fibrils divided by the total cross-sectional area of the nerve. Each fibril was treated as a linear elastic member in tension. As the simulation progressed, the force contribution from each fibril in the axial direction was computed as the cosine of the angle it made with the nerve axis. Fibrils were assigned a Poisson's ratio of 0.5, to calculate stress in the fibril at the high induced strains. Also, the whole nerve was assigned a Poisson's ratio of 0.5, and stress in the nerve was calculated as the sum of the forces in the fibrils divided by the cross-sectional area of the nerve at that point in the simulation in order to maintain a true-stress/true-strain formulation.

Upon reaching their ultimate tensile strength as prescribed by a Weibull distribution (described below) individual fibrils reaching their rupture load were removed, and no longer contributed to the tensile force. Thus, the nonlinear and highly stochastic failure response observed in our experimental data [32] was effectively modeled using elastic elements with initial waviness and a stochastic failure criterion. Nonlinearity in the failure region is distinct from nonlinearity of the toe region; the latter results only from fibril straightening, as depicted in Fig. 7(*b*). Indeed, strains of up to 10% frequently were applied before some of the fibrils become straight and contributed to the axial stress in our simulations, using realistic geometries. The combined contributions of waviness and stochastic failure to nonlinearity in these simulated stress–strain curves resulted in total simulation strains of 0.4–0.5, as compared with typical fibril failure strains which were on the order of 0.10–0.20.

Subsequent to finding the combination of $\bar{a}$, and σ_a, or $\bar{a}$ and σ_γ, that minimized the RMS error as defined above, the Weibull parameters α and x_0 were found using a similar RMS-minimization method as for the toe region. In order to ensure independence between geometry and strength parameters, sets of ten simulations were spawned in a grid-like fashion for each combination of Weibull parameters α and x_0. To make the model dimensionless we used

$$E_{x_i} = \frac{x_0}{E_{f_i}}, \tag{15}$$

where $E_{x_i} \in (0.1,0.15,0.2,\ldots,2.0)$ is the Weibull scale parameter, x_0, of the *i*th fibril normalized to E_{f_i}, the modulus of the *i*th fibril. A set of random numbers $(0 < x_i < 1)$ were transformed to ultimate tensile strengths, U_i, via Weibull parameters, α and x_0, by solving the Weibull cumulative distribution function

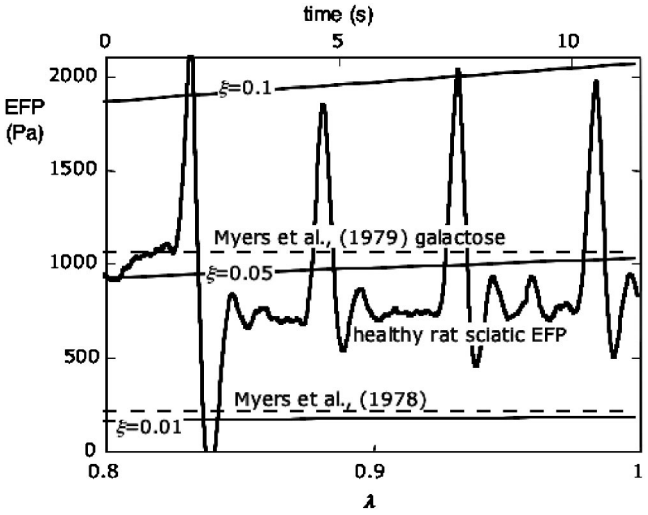

Fig. 8 A parametric plot of endoneurial fluid pressure (EFP) as a function of dimensionless parameters η and ξ, Eq. (8). Superimposed is an endoneurial fluid pressure trace recorded from a healthy BioBreeding rat [32]. Data taken with a 900A microfluidic pressure-device (World Precision Instruments, Sarasota, FL).

$$F(x_i) = 1 - e^{-(U_i/x_0)^\alpha}. \tag{16}$$

for U_i

$$U_i = x_0(-\ln(1-x_i))^{1/\alpha}. \tag{17}$$

The Weibull shape parameter α was also mapped over the domain $\alpha \in (0.1,0.15,0.2,\ldots,2.0)$. This range was sufficient to find the RMS minimum value "valley" for the difference between experimental and simulated stress–strain curves that included the entire failure curve from toe region to failure.

Prior SEM results have shown that individual collagen fibrils frequently cross into different bundles along their axes [46,60]; thus, selection of a specific assumption for load sharing within a bundle is somewhat problematic. Here, we investigated the two extrema in load sharing: equal load sharing (ELS), wherein unbroken fibers in a bundle share load equally [86], and immediate-neighbor local load sharing (LLS), wherein only the unbroken fibers adjacent to broken fibers in a bundle are subject to overload. One LLS scenario formulated by Harlow and Phoenix [77] scaled overload on unbroken fibers by their proximity to broken fibers, per

$$K_{r_i} = 1 + r/2, \tag{18}$$

where K_{r_i} is the stress concentration factor of the ith fibril and r is the number of broken fibrils adjacent to it. This rule preserves equilibrium, as

$$\sum_{i=1}^{NF} K_{r_i} = NF. \tag{19}$$

It is convenient to assume that fibers are arranged in a circular array in this model, as per Harlow and Phoenix [77]. We give simple example for 11 fiber arrays, for equal and local load sharing. Initially, in both scenarios, each fiber bears an equal fraction of a unit load (1/11). For equal load sharing, the first fiber failure increases the other fibrils' loads to 1/10. For local load sharing, the first fiber failure produces overloads on its two nearest neighbors only, which each receive a load of one and a half times their original load (3/22); the eight intact fibers maintain their load of 1/11.

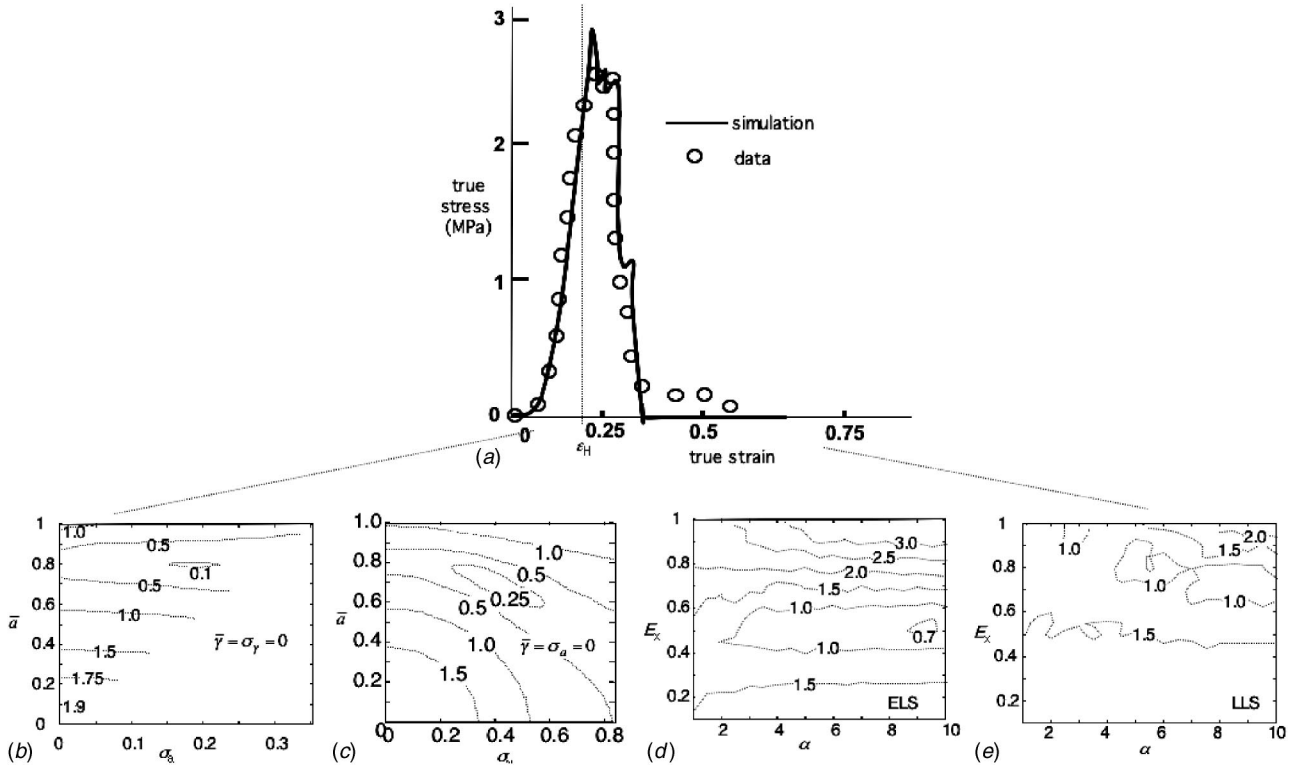

Fig. 9 Example of fitting of experimental stress–strain-failure data from the sciatic nerve of a healthy (nondiabetic) BioBreeding rat (lab designation 018-60-16). Initially, (*a*) simulated data are superimposed on experimental data [32], (*b*) parametric plot of RMS error as a function of average fibril amplitude, $\bar{a}$, and fibril amplitude standard deviation, σ_a, and (*c*) parametric plot of RMS error as a function of average fibril amplitude, $\bar{a}$, and fibril angle standard deviation, σ_γ, parametric contour plots of RMS error as a function of Weibull shape parameter, α, and normalized Weibull scale parameter, E_x ($E_x = E_f / x_0$) E_f=average fibril modulus, x_0=Weibull scale parameter for (*d*) equal load sharing and (*e*) local load sharing.

Methods: Experimental

Endoneurial Fluid Pressure. Study animals were cared for and euthanized in accordance with University, State, and Federal standards, and with the National Research Council's "Guide for the Care and Use of Laboratory Animals." To obtain EFP in living rats, a microfluidic pressure transducer (900A, World Precision Instruments, Sarasota, FL) was used. After dosing with 150 mg/kg of sodium pentobarbitol, rats were tested for anesthesia. Right sciatic nerves were then exposed. A 1.0 M NaCl solution was used in a 5 μm glass micropipette tip to transduce hydrodynamic pressure. Data were collected at a sample rate of 250 Hz. The accuracy of the instrument was ~100 Pa with a stability of 0.1 mmHg (13 Pa) and was transduced at 10 mV/mmHg (10 mV/133 Pa). Prior to *in vivo* measurement, the device was calibrated in a static column of 0.1 M NaCl. The signal was stored digitally using LabView software (National Instruments) running on a PC (Dell). EFP was determined by averaging of the signal.

Uniaxial Testing. Mechanical tests on whole nerve [32] were used for comparison with our simulation results. Specimens used for mechanical testing were obtained from healthy and diabetic rats. Nerves were dissected from sacrificed rats, and thawed at room temperature for approximately five minutes, then clamped in a pin-and-groove grip, affixed to an Ohaus digital scale (model TP2KS). Strain was applied using a Bodine Electric Company DC stepper motor controlled by a Parker Digiplan PK3 driver. An interclamp length of 10 mm and displacement rate of 0.1 mm/s (strain rate 0.01/s) were used. Zero strain was defined as the point at which a force of 2.0×10^{-5} N was detected. Nerves were strained until failure occurred. Data were collected at a rate of 1 Hz and stored on an Apollo Domain Series 4000 digital computer. Prior to mechanical testing, five cross sections were measured and averaged for data reduction using NIH image analyses of SPOT RT II digital camera section images. Nerves were not preconditioned.

Results

Pressure-Vessel Representation of Peripheral Nerve. Figure 8 shows a plot of Eq. (8) with ξ=(0.01,0.05,0.1), η=0.02, E_{zz}=0.5 MPa, $\lambda \in (0.8-1.0)$, β=0. We see that the deformation observed upon peripheral nerve extraction agrees well with literature values. Note that we have superimposed endoneurial fluid pressure recorded from the sciatic nerve contralateral to the one used for uniaxial testing. This previously unpublished data was obtained in our laboratory from a live healthy BioBreeding rat under anesthesia according to the protocol of Myers et al. [79,80] as described above.

RMS Minimization Results for Toe Region. A typical stress–strain curve to failure is shown in Fig. 9(*a*), for a control rat sciatic nerve. The toe, linear, failure and post-failure portions of the curve are clearly distinguishable for both the experimental and theoretical curves. In comparing simulation results with experimental results, we found combinations of either $(\bar{a},\sigma_a)$ or $(\bar{a},\sigma_\gamma)$ that minimized RMS error between experimental and simulated data (Fig. 9(*b*)). Figure 9(*b*) shows a minimum value, per the RMS "valley" near $\bar{a}$=0.8, σ_a=0.2. Combinations of $\bar{a}$ and σ_a wherein both values are smaller exhibit smaller toe regions; combinations wherein both are greater exhibit more extensive toe regions.

RMS Minimization Results for Full Stress–Strain Curve. After the toe region was matched, and using the combination of $\bar{a}$ and σ_a that minimized the RMS error for that region, RMS error

was minimized for the remainder of the failure curve using trial combinations of α and E_x (Fig. 9(*c*,*d*)). As in the case of toe region matching, where a RMS "valley" was found, regions of minimum error were also found for both ELS and LLS. For this particular tissue specimen, a combination of $E_x=0.5$ and $\alpha=9.0$ gave the minimum RMS error, whereas for LLS loading, the error valley was not as well defined.

Equal Versus Local Load Sharing Among Elastic Fibers. Local and equal load sharings are compared in Fig. 9(*c*,*d*), which demonstrates that local load sharing results in greater variability in strength, stiffness, and thus in fitted geometric parameters. Also, assumed in-plane interactions among fibrils, requires that fibrils be stronger, as evidenced by a greater E_x and have Weibull scale parameter β in order to produce tissue strength equivalent to an ELS array.

The small pocket of low RMS error near $E_x=1$, $\alpha=3$ implies that there is not a unique arrangement which results in mechanical integrity: a broader Weibull distribution function (lower shape parameter, α) with a high fraction of both weak and strong fibrils requires that the strongest fibrils be stronger than in a situation where the Weibull distribution is narrow (larger shape parameter, α).

Discussion

Scalability of Collagen Model. This approach allows for scalability, via a function that models a fibrous material as a chain, or connected series, of intact bundles. Use of the exponential Weibull distribution function results in linear increases in the strength of fibrils or inter-fibril bonds with multiplicative increases in the number of fibrils per unit length. For example, if it were found that fibril lengths were actually one half of the lengths assumed here, a resultant increase in fibril strength of 10 MPa would be predicted.

Isolation of Geometry From Mechanical Modeling. The gross mechanical properties of peripheral nerve are well documented [57,56], and the mechanical properties of single collagen fibrils have also been measured [84]. The pressure vessel model was developed primarily to verify that our observed moduli were consistent with previous results of EFP experiments. This was indeed the case since our tow-region modulus was 2–3 orders of magnitude lower than the linear region.

The significant discrepancy between the fibril modulus used here, of 336 MPa, and that of 5 GPa found recently for rat tail collagen fibrils [87], may be due to molecular differences in the two tissues, or due the fact that both our method and that of Silver et al., [87] are indirect and likely subject to revision, once methods for testing smaller samples become available. The fibrillar collagen content of a peripheral nerve has been determined more reliably [35,88], and collagen fibril diameter distributions have also been reported [5–7]. Several workers have suggested that mechanics play a role in the permanence of diabetic peripheral neuropathy [5,89]. The tissue-scale morphology of the collagen fibril bundle arrangement is summarized by essentially six sources [46,90–94]. Of these only Stolinski [90], Ushiki and Ide [46] and Haninec [93], imaged epineurium, and none of the authors made an attempt to fully quantify collagen fibril bundle periodicity.

Since statistics for both normalized fibril amplitude, a, and fibril angle, γ, are likely to affect toe-region shape independently, we treated them as such in a series of simulations where $\bar{a}$ varied from 0 to 1 in increments of 0.025 and σ_γ varied from 0 to ~0.85 in 40 increments. This range was found to be sufficient to cover the entire range to capture the minimum RMS error between simulated and experimental curves. Our strategy was to run simulations only up to ε_H to fit the variables $\bar{a}$ and σ_a in one simulation set then find combinations of $\bar{a}$ and σ_γ to find the minimum RMS error in a second simulation set. In this manner, we were assured of bounding all reasonable values of our geometry variables. Per Fig. 9, there are clearly several combinations of variables, for example, $\bar{a}$ and σ_a or $\bar{a}$ and σ_γ that map to a given RMS errors. For the two domain variables, $\bar{a}$ and σ_a or $\bar{a}$ and σ_γ, the RMS error is single-valued, however, and we have bounded the combinations of these variables that contain the minimum value to within 2.5% (40 values per axis) of the range of values of physiological significance for this tissue. The contour maps of RMS error as a function of E_x and α, on the other hand, are more convoluted, but appear nonetheless single-valued for each combination of E_x and α. Additional realizations of these simulations could be expected to produce slightly different results, but again, the regions of the solution-space which contain the RMS minimum to a precision of 2.5% of the relevant scale have been apparently isolated.

Implications of Material Stress Concentrations on Fibroblast and Perineurial Cell Loads. The importance of local stresses and the general properties of these materials cannot be overstated, both for gaining fundamental understanding of physiological loads and tissue remodeling in response to loads, and also design of artificial tissues. Recent studies of forces generated at the cellular scale by perineurial cells [95] hint at local stresses, but still need to be corroborated with global hoop stresses on the order of 1 MPa [74] and global axial stresses on the order of 10 MPa [96]. Many workers are presently interested in physiological load conditions, but stochastic construction is a key feature of the morphology of biomaterials, and is the primary motivation for the present study.

Several authors have attempted to correlate mechanical stress at the cellular level with increased extracellular matrix production [97,98]. Perineurial cells have also been shown to express fibrillar collagen [68,99], and may respond in a similar manner to fibroblasts when mechanically stressed. Our results suggest that for heavily glycated (crosslinked) tissues, the in-plane loads between ECM-producing cells such as fibroblasts and perineurial cells and the extracellular matrix that surrounds them, may be enhanced and thus drive up ECM protein expression [63,98]. The exact pathways and a quantifiable in vivo function of expression as a function of load has not been established, but more than likely involves signaling between extracellular matrix and cytoskeletal proteins [98].

We believe that our model will be useful in characterizing other peripheral nerve tissues of a similar anatomy to the rat sciatic nerve, including human tissues. Patient-specific connective tissue distributions could be determined via the AFM of needle-punch specimens, to provide input to our models, in order to allow a prediction of the effect of alterations in the extracellular matrix on the overall mechanical response. The limitations of our model include our incomplete understanding of the factors affecting collagen fibril crosslinking, and the effect of disease or injury on this crosslinking. Correlative studies are needed, in conjunction with improved imaging technologies (both physical and immunohistochemical) to provide data for input to our models, in order to realize possible benefits.

Conclusions and Summary

With this work we have identified some of the key parameters responsible for the mechanical behavior of peripheral nerve, starting at the tissue scale of whole nerve, where endoneurial fluid pressures on the order of kilopascals, and *in vivo* stresses on the order of megapascals play a role. From our model, we have correlated the estimated fibril geometry and strength, and interfibrillar connectivity. Fibril amplitudes, angles and strengths in the collagens of a peripheral nerve clearly dictate the shape and extent of the toe region. Fibril amplitudes of approximately 0.8 fit experimental toe regions. This is larger than those that may be approximated from the most exhaustive SEM images of the literature (~0.4–0.5) [46]. By an additional consideration of the fibril axial angle, this value dropped to 0.6–0.7 (Fig. 9(*c*)). Clearly, in order for the nerve to maintain mechanical integrity under normal

physiological deformations, collagen fibrils must be angled. This may partially be the role of the tight-junction-connected perineurial cells, but the relative contributions remains to be determined. Use of this model in investigating possible crosslink density changes and local loads in the peripheral nerve will be part of future investigations.

Acknowledgment

This work was supported by the Whitaker Foundation, the DARPA Synthetic Multifunctional Materials Program (Dr. Leo Christodoulou and Dr. Steve Fishman, program monitors) and by a NSF PECASE grant (Sastry). This support is gratefully acknowledged.

Nomenclature

$\overline{a}$ = average fibril amplitude
A = lower limit of integration for sinusoidal fibril
A_0 = initial cross-sectional area
A_f = final cross-sectional area
f_c = collagenous area fraction of nerve (dimensionless)
f_p = packing area fraction of collagen in collagenous portion of nerve (dimensionless)
B = upper limit of integration for sinusoidal fibril
d_f = collagen fibril diameter
E_f = average fibril modulus
E_{x_i} = Weibull scale parameter normalized to fibril modulus
E_{zz} = axial epineurial/perineurial modulus
$E_{\theta\theta}$ = circumferential epineurial/perineurial modulus
f_p = packing fraction of collagen within collagenous portion of nerve
K_{r_i} = stress concentration factor of the *i*th fibril
L' = fibril length at which fibril becomes straight
L_0 = *in vivo* epineurial/perineurial length
L_f = final length
L_p = *ex vivo* epineurial/perineurial length
N_a = scaling coefficient for fibril amplitude normal distribution
NF = number of fibrils in simulation
N_0 = normalization scaling coefficient for fibril amplitude normal distribution
N_γ = scaling coefficient for fibril angle normal distribution
p = hydrostatic endoneurial fluid pressure
s = curvilinear path of sinusoidal fibril
t = epineurial/perineurial thickness
U_i = fibril ultimate tensile strength
x_i = equally spaced seed variables for generating distribution functions
x_0 = Weibull scale parameter
α = Weibull shape parameter
β = epineurial/perineurial ex vivo/in vivo diameter ratio
$\varepsilon_\square$ = greatest strain of linear portion of whole nerve stress-strain curve
ε_L = least strain of linear portion of whole nerve stress-strain curve
$\varepsilon_{\theta\theta}$ = circumferential epineurial/perineurial strain
Φ = normal distribution function
ϕ_0 = in vivo endoneurial diameter
ϕ_p = ex vivo epineurial/perineurial diameter
γ = average fibril angle
η = t/ϕ_e
λ = Lp/L0 epineurial/perineurial in vivo/ex vivo length ratio
$\nu_{z\theta}$ = axial-circumferential epineurial/perineurial Poisson's ratio
$\nu_{\theta z}$ = circumferential-axial epineurial/perineurial Poisson's ratio
σ_a = fibril amplitude standard deviation
σ_E = engineering stress
σ_H = greatest stress of linear portion of whole nerve stress–strain curve
σ_L = least stress of linear portion of whole nerve stress–strain curve
σ_T = true stress
σ_γ = fibril angle standard deviation
$\sigma_{\theta\theta}$ = circumferential epineurial/perineurial stress
σ_{zz} = axial epineurial/perineurial stress
ξ = $E_{\theta\theta}/E_{zz}$ ratio between epineurial/perineurial moduli

References

[1] Myllyharju, J., and Kivirikko, K. I., 2001, ''Collagens and Collagen-Related Diseases,'' Ann. Med., **33**, pp. 7–21.
[2] Prockop, D. J., and Kivirikko, K. I., 1995, ''Collagens: Molecular Biology, Diseases, and Potentials for Therapy,'' Annu. Rev. Biochem., **64**, pp. 403–434.
[3] Vandenberg, P., 1993, ''Molecular Basis of Heritable Connective Tissue Disease,'' Biochem. Med. Metab. Biol., **49**, pp. 1–12.
[4] Benjamin, I. J., 2001, ''Matrix Metalloproteinases: From Biology to Therapeutic Strategies in Cardiovascular Disease,'' J. Investig. Med., **49**, pp. 381–397.
[5] Bradley, J. L., King, R. H., Muddle, J. R., and Thomas, P. K., 2000, ''The Extracellular Matrix of Peripheral Nerve in Diabetic Polyneuropathy,'' Acta Neuropathol. (Berl), **99**, pp. 539–546.
[6] Muona, P., Jaakkola, S., Salonen, V., and Peltonen, J., 1989, ''Diabetes Induces the Formation of Large Diameter Collagen Fibrils in the Sciatic Nerves of BB Rats,'' Matrix, **9**, pp. 62–67.
[7] Wang, H., Layton, B. E., and Sastry, A. M., 2003, ''Nerve Collagens From Diabetic and Non-Diabetic Sprague-Dawley and BioBreeding Rats: An Atomic Force Microscopy Study,'' Diabetes/Metab. Rev., **19**, pp. 288–98.
[8] Perkins, B. A., and Bril, V., 2002, ''Diagnosis and Management of Diabetic Neuropathy,'' Curr. Diabetes Rep., **2**, pp. 495–500.
[9] Ephraim, P. L., Dillingham, T. R., Sector, M., Pezzin, L. E., and Mackenzie, E. J., 2003, ''Epidemiology of Limb Loss and Congenital Limb Deficiency: A Review of the Literature,'' Arch. Phys. Med. Rehabil., **84**, pp. 747–761.
[10] Poncelet, A. N., 2003, ''Diabetic Polyneuropathy, Risk Factors, Patterns of Presentation, Diagnosis, and Treatment,'' Geriatrics, **58**, pp. 16–18, 24–15, 30.
[11] Rittie, L., Berton, A., Monboisse, J. C., Hornebeck, W., and Gillery, P., 1999, ''Decreased Contraction of Glycated Collagen Lattices Coincides With Impaired Matrix Metalloproteinase Production,'' Biochem. Biophys. Res. Commun., **264**, pp. 488–492.
[12] Thornalley, P. J., 2002, ''Glycation in Diabetic Neuropathy: Characteristics, Consequences, Causes, and Therapeutic Options,'' Int. Rev. Neurobiol., **50**, pp. 37–57.
[13] Vasan, S., Zhang, X., Kapurniotu, A., Bernhagen, J., Teichberg, S., Basgen, J., Wagle, D., Shih, D., Terlecky, I., Bucala, R., Cerami, A., Egan, J., and Ulrich, P., 1996, ''An Agent Cleaving Glucose-Derived Protein Crosslinks In Vitro and In Vivo,'' Nature (London), **382**, pp. 275–278.
[14] Haftek, J., 1970, ''Stretch Injury of Peripheral Nerve,'' J. Bone Jt. Surg., **52B**, pp. 354–365.
[15] Robinson, L. R., 2000, ''Traumatic Injury to Peripheral Nerves,'' Muscle Nerve, **23**, pp. 863–873.
[16] Ahmed, N., Argirov, O. K., Minhas, H. S., Cordeiro, C. A., and Thornalley, P. J., 2002, ''Assay of Advanced Glycation Endproducts (AGEs): Surveying AGEs by Chromatographic Assay With Derivatization by 6-Aminoquinolyl-N-Hydroxysuccinimidyl-Carbamate and Application to Nepsilon-Carboxymethyl-Lysine- and Nepsilon-(1-Carboxyethyl)Lysine-Modified Albumin,'' Biochem. J., **364**, pp. 1–14.
[17] Yang, S., Litchfield, J. E., and Baynes, J. W., 2003, ''AGE-Breakers Cleave Model Compounds, But Do Not Break Maillard Crosslinks in Skin and Tail Collagen From Diabetic Rats,'' Arch. Biochem. Biophys., **412**, pp. 42–46.
[18] Lundborg, G., 1988, ''Intraneural Microcirculation,'' Orthop. Clin. North Am., **19**, pp. 1–12.
[19] Kalichman, M. W., and Myers, R. R., 1991, ''Transperineurial Vessel Constriction in an Edematous Neuropathy,'' J. Neuropathol. Exp. Neurol., **50**, pp. 408–418.
[20] Dumanian, G. A., McClinton, M. A., and Brushart, T. M., 1999, ''The Effects of Free Grafts on the Stiffness of the Rat Sciatic Nerve and Perineurial Scar,'' J. Hand Surg. [Am], **24**, pp. 30–36.
[21] Thomas, P. K., Berthold, C. H., and Ochoa, J., 1993, ''Microscopic Anatomy of the Peripheral Nervous System,'' in *Peripheral Neuopathy*, P. J. Dyck, P. K. Thomas, J. W. Griffin, P. A. Low, and J. F. Poduslo, eds., Saunders, Philadelphia, pp. 28–90.
[22] Thomas, E., and Sourander, P., 1977, ''Impaired Development of the Rat Perineurium by Undernutrition. An Enzyme Histochemical Study,'' Acta Neuropathol. (Berl), **38**, pp. 77–80.
[23] Myers, R. R., Heckman, H. M., and Powell, H. C., 1983, ''Endoneurial Fluid is Hypertonic,'' J. Neuropathol. Exp. Neurol., **42**, pp. 217–224.
[24] Thomas, P. K., 1963, ''The Connective Tissue of the Peripheral Nervous System,'' J. Anat., **97**, pp. 35–44.
[25] Gefen, A., Megido-Ravid, M., Azariah, M., Itzchak, Y., and Arcan, M., 2001, ''Integration of Plantar Soft Tissue Stiffness Measurements in Routine MRI of the Diabetic Foot,'' Clin. Biomech. (Los Angel. Calif.), **16**, pp. 921–925.
[26] Gefen, A., 2003, ''Plantar Soft Tissue Loading Under the Medial Metatarsals

in the Standing Diabetic Foot,'' Med. Eng. Phys., **25**, pp. 491–499.
[27] Reihsner, R., and Menzel, E. J., 1998, ''Two-Dimensional Stress–Relaxation Behavior of Human Skin as Influenced by Non-Enzymatic Glycation and the Inhibitory Agent Aminoguanidine,'' J. Biomech., **31**, pp. 985–993.
[28] Reihsner, R., Melling, M., Pfeiler, W., and Menzel, E. J., 2000, ''Alterations of Biochemical and Two-Dimensional Biomechanical Properties of Human Skin in Diabetes Mellitus as Compared to Effects of In Vitro Non-Enzymatic Glycation,'' Clin. Biomech. (Los Angel. Calif.), **15**, pp. 379–386.
[29] Shoemaker, P. A., Schneider, D., Lee, M. C., and Fung, Y. C., 1986, ''A Constitutive Model for Two-Dimensional Soft Tissues and Its Application to Experimental Data,'' J. Biomech., **19**, pp. 695–702.
[30] Haut, R. C., and Little, R. W., 1972, ''A Constitutive Equation for Collagen Fibers,'' J. Biomech., **5**, pp. 423–430.
[31] Provenzano, P., Lakes, R., Keenan, T., and Vanderby, Jr., R., 2001, ''Nonlinear Ligament Viscoelasticity,'' Ann. Biomed. Eng., **29**, pp. 908–914.
[32] Layton, B. E., Sastry, A. M., Wang, H., Sullivan, K. A., Feldman, E. L., Komorowski, T. E., and Philbert, M. A., 2004, ''Differences Between Sciatic Nerve Collagen Morphologies, Properties and Distribution in Diabetic and Normal BioBreeding and Sprague-Dawley Rat Nerves,'' J. Biomech., (accepted).
[33] Myers, R. R., and Powell, H. C., 1984, ''Galactose Neuropathy: Impact of Chronic Endoneurial Edema on Nerve Blood Flow,'' Ann. Neurol., **16**, pp. 587–594.
[34] Myers, R. R., Murakami, H., and Powell, H. C., 1986, ''Reduced Nerve Blood Flow in Edematous Neuropathies: A Biomechanical Mechanism,'' Microvasc. Res., **32**, pp. 145–151.
[35] Seyer, J. M., Kang, A. H., and Whitaker, J. N., 1977, ''The Characterization of Type I and Type III Collagens From Human Peripheral Nerve,'' Biochim. Biophys. Acta, **492**, pp. 415–425.
[36] Podratz, J. L., Rodriguez, E., and Windebank, A. J., 2001, ''Role of the Extracellular Matrix in Myelination of Peripheral Nerve,'' Glia, **35**, pp. 35–40.
[37] Williams, P. W., Lowry, A., Hill, R., and Masson, E., 2000, ''Relationship Between Fascicle Size and Perineurial Collagen IV Content in Diabetic and Control Human Peripheral Nerve,'' Histopathology, **36**, pp. 551–555.
[38] Lowry, A., Wilcox, D., Masson, E. A., and Williams, P. E., 1997, ''Immunohistochemical Methods for Semiquantitative Analysis of Collagen Content in Human Peripheral Nerve,'' J. Anat., **191**, pp. 367–374.
[39] Peltonen, J., Kahari, L., Uitto, J., and Jimenez, S. A., 1990, ''Increased Expression of Type VI Collagen Genes in Systemic Sclerosis,'' Arthritis Rheum., **33**, pp. 1829–1835.
[40] Carbonetto, S., 1984, ''The Extracellular Matrix of the Nervous System,'' Trends Neurosci., **7**, pp. 382–387.
[41] Shellswell, G. B., Restall, D. J., Duance, V. C., and Bailey, A. J., 1979, ''Identification and Differential Distribution of Collagen Types in the Central and Peripheral Nervous System,'' FEBS Lett., **106**, pp. 305–308.
[42] Salonen, V., Lehto, M., Vaheri, A., Aro, H., and Peltonen, J., 1985, ''Endoneurial Fibrosis Following Nerve Transection—An Immunohistological Study of Collagen Types and Fibronectin in the Rat,'' Hum. Gene Ther., **67**, pp. 315–321.
[43] Lorimer, P., Mezin, P., Moleur, F. L., Pinel, N., Peyrol, S., and Stoebner, P., 1992, ''Ultrastructural Localization of the Major Components of the Extracellular Matrix in Normal Rat Nerve,'' J. Histochem. Cytochem., **40**, pp. 859–868.
[44] Fleischmajer, R., Timpl, R., Dziadek, M., and Lebwohl, M., 1985, ''Basement Membrane Proteins Interstitial Collagens, and Fibronectin in Neurofibroma,'' J. Invest. Dermatol., **85**, pp. 54–59.
[45] Sullivan, K. A., 2003, private communication.
[46] Ushiki, T., and Ide, C., 1990, ''Three-Dimensional Organization of the Collagen Fibrils in the Rat Sciatic Nerve as Revealed by Transmission- and Scanning Electron Microscopy,'' Cell Tissue Res., **260**, pp. 175–184.
[47] Holmes, D. F., Graham, H. K., Trotter, J. A., and Kadler, K. E., 2001, ''STEM/TEM Studies of Collagen Fibril Assembly,'' Micron, **32**, pp. 273–285.
[48] Birk, D. E., Zycband, E. I., Woodruff, S., Winkelmann, D. A., and Trelstad, R. L., 1997, ''Collagen Fibrillogenesis In Situ: Fibril Segments Become Long Fibrils as the Developing Tendon Matures,'' Dev. Dyn., **208**, pp. 291–298.
[49] Ottani, V., Raspanti, M., and Ruggeri, A., 2001, ''Collagen Structure and Functional Implications,'' Micron, **32**, pp. 251–260.
[50] Muona, P., Peltonen, J., Jaakkola, S., and Uitto, J., 1991, ''Increased Matrix Gene Expression by Glucose in Rat Neural Connective Tissue Cells in Culture,'' Diabetes, **40**, pp. 605–611.
[51] Odetti, P., Aragno, I., Rolandi, R., Garibaldi, S., Valentini, S., Cosso, L., Traverso, N., Cottalasso, D., Pronzato, M. A., and Marinari, U. M., 2000, ''Scanning Force Microscopy Reveals Structural Alterations in Diabetic Rat Collagen Fibrils: Role of Protein Glycation,'' Diabetes/Metab. Rev., **16**, pp. 74–81.
[52] Tanaka, S., Avigad, G., Brodsky, B., and Eikenberry, E. F., 1988, ''Glycation Induces Expansion of the Molecular Packing of Collagen,'' J. Mol. Biol., **203**, pp. 495–505.
[53] Hulmes, D. J., 2002, ''Building Collagen Molecules, Fibrils, and Suprafibrillar Structures,'' J. Struct. Biol., **137**, pp. 2–10.
[54] Feldman, E. L., 2003, ''Oxidative Stress and Diabetic Neuropathy: A New Understanding of an Old Problem,'' J. Clin. Invest., **111**, pp. 431–433.
[55] Russell, J. W., Golovoy, D., Vincent, A. M., Mahendru, P., Olzmann, J. A., Mentzer, A., and Feldman, E. L., 2002, ''High Glucose-Induced Oxidative Stress and Mitochondrial Dysfunction in Neurons,'' FASEB J., **16**, pp. 1738–1748.
[56] Wall, E. J., Kwan, M. K., Rydevik, B. L., Woo, S. L., and Garfin, S. R., 1991, ''Stress Relaxation of a Peripheral Nerve,'' J. Hand Surg. [Am], **16**, pp. 859–863.
[57] Abrams, R. A., Butler, J. M., Bodine-Fowler, S., and Botte, M. J., 1998, ''Tensile Properties of the Neurorrhaphy Site in the Rat Sciatic Nerve,'' J. Hand Surg. [Am], **23**, pp. 465–470.
[58] Toby, E. B., Rotramel, J., Jayaraman, G., and Struthers, A., 1999, ''Changes in the Stress Relaxation Properties of Peripheral Nerves After Transection,'' J. Hand Surg. [Am], **24**, pp. 694–699.
[59] Roeder, B. A., Kokini, K., Sturgis, J. E., Robinson, J. P., and Voytik-Harbin, S. L., 2002, ''Tensile Mechanical Properties of Three-Dimensional Type I Collagen Extracellular Matrices With Varied Microstructure,'' ASME J. Biomech. Eng., **124**, pp. 214–222.
[60] Parry, D. A., 1988, ''The Molecular and Fibrillar Structure of Collagen and Its Relationship to the Mechanical Properties of Connective Tissue,'' Biophys. Chem., **29**, pp. 195–209.
[61] Hurschler, C., Loitz-Ramage, B., and Vanderby, Jr., R., 1997, ''A Structurally Based Stress–Stretch Relationship for Tendon and Ligament,'' ASME J. Biomech. Eng., **119**, pp. 392–399.
[62] Sacks, M. S., 2003, ''Incorporation of Experimentally Derived Fiber Orientation Into a Structural Constitutive Model for Planar Collagenous Tissues,'' ASME J. Biomech. Eng., **125**, pp. 280–287.
[63] Kessler, D., Dethlefsen, S., Haase, I., Plomann, M., Hirche, F., Krieg, T., and Eckes, B., 2001, ''Fibroblasts in Mechanically Stressed Collagen Lattices Assume a 'Synthetic' Phenotype,'' J. Biol. Chem., **276**, pp. 36575–36585.
[64] Benazzoug, Y., Borchiellini, C., Labat-Robert, J., Robert, L., and Kern, P., 1998, ''Effect of High-Glucose Concentrations on the Expression of Collagens and Fibronectin by Fibroblasts in Culture,'' Exp. Gerontol., **33**, pp. 445–455.
[65] Hadley, J., Malik, N., and Meek, K., 2001, ''Collagen as a Model System to Investigate the Use of Aspirin as an Inhibitor of Protein Glycation and Crosslinking,'' Micron, **32**, pp. 307–315.
[66] Malik, N. S., Moss, S. J., Ahmed, N., Furth, A. J., Wall, R. S., and Meek, K. M., 1992, ''Ageing of the Human Corneal Stroma: Structural and Biochemical Changes,'' Biochim. Biophys. Acta, **1138**, pp. 222–228.
[67] Sajithlal, G. B., Chithra, P., and Chandrakasan, G., 1998, ''Advanced Glycation End Products Induce Crosslinking of Collagen In Vitro,'' Biochim. Biophys. Acta, **1407**, pp. 215–224.
[68] Peltonen, J. T., Kalliomaki, M. A., and Muona, P. K., 1997, ''Extracellular Matrix of Peripheral Nerves in Diabetes,'' J. Peripher Nerv. Syst., **2**, pp. 213–226.
[69] Rempel, D., Dahlin, L., and Lundborg, G., 1999, ''Pathophysiology of Nerve Compression Syndromes: Response of Peripheral Nerves to Loading,'' J. Bone Jt. Surg., Am. Vol., **81**, pp. 1600–1610.
[70] Mackinnon, S. E., 2002, ''Pathophysiology of Nerve Compression,'' Hand Clin., **18**, pp. 231–241.
[71] Simmons, Z., and Feldman, E. L., 2002, ''Update on Diabetic Neuropathy,'' Curr. Opin. Neurol., **15**, pp. 595–603.
[72] Reed, N., and Gutmann, D. H., 2001, ''Tumorigenesis in Neurofibromatosis: New Insights and Potential Therapies,'' Trends Mol. Med., **7**, pp. 157–162.
[73] Low, P. A., Dyck, P. J., and Schmelzer, J. D., 1980, ''Mammalian Peripheral Nerve Sheath Has Unique Responses to Chronic Elevations of Endoneurial Fluid Pressure,'' Exp. Neurol., **70**, pp. 300–306.
[74] Low, P. A., 1981, ''In Vitro Study of Acute Elevations of Endoneurial Pressure in Mammalian Peripheral Nerve Sheath,'' Exp. Neurol., **74**, pp. 160–169.
[75] Ask, P., Levitan, H., Robinson, P. J., and Rapoport, S. I., 1983, ''Peripheral Nerve as an Osmometer: Role of the Perineurium in Frog Sciatic Nerve,'' Am. J. Physiol., **244**, pp. C75–81.
[76] Rydevik, B. L., Kwan, M. K., Myers, R. R., Brown, R. A., Triggs, K. J., Woo, S. L., and Garfin, S. R., 1990, ''An In Vitro Mechanical and Histological Study of Acute Stretching on Rabbit Tibial Nerve,'' J. Orthop. Res., **8**, pp. 694–701.
[77] Harlow, D. G., and Phoenix, S. L., 1978, ''Chain-of-Bundles Probability Model for Strength of Fibrous Materials .1. Analysis and Conjectures,'' J. Compos. Mater., **12**, pp. 195–214.
[78] de Medinaceli, L., Leblanc, A. L., and Merle, M., 1997, ''Functional Consequences of Isolated Nerve Stretch: Experimental Long-Term Static Loading,'' J. Reconstr Microsurg, **13**, pp. 185–192.
[79] Myers, R. R., Powell, H. C., Costello, M. L., Lampert, P. W., and Zweifach, B. W., 1978, ''Endoneurial Fluid Pressure: Direct Measurement With Micropipettes,'' Brain Res., **148**, pp. 510–515.
[80] Myers, R. R., Costello, M. L., and Powell, H. C., 1979, ''Increased Endoneurial Fluid Pressure in Galactose Neuropathy,'' Muscle Nerve, **2**, pp. 299–303.
[81] Parkinson, J., Brass, A., Canova, G., and Brechet, Y., 1997, ''The Mechanical Properties of Simulated Collagen Fibrils,'' J. Biomech., **30**, pp. 549–554.
[82] Pins, G. D., Christiansen, D. L., Patel, R., and Silver, F. H., 1997, ''Self-Assembly of Collagen Fibers. Influence of Fibrillar Alignment and Decorin on Mechanical Properties,'' Biophys. J., **73**, pp. 2164–2172.
[83] Christiansen, D. L., Huang, E. K., and Silver, F. H., 2000, ''Assembly of Type I Collagen: Fusion of Fibril Subunits and the Influence of Fibril Diameter on Mechanical Properties,'' Matrix Biol., **19**, pp. 409–420.
[84] Sasaki, N., and Odajima, S., 1996, ''Stress–Strain Curve and Young's Modulus of a Collagen Molecule as Determined by the X-Ray Diffraction Technique,'' J. Biomech., **29**, pp. 655–658.
[85] http://www.vni.com, August, 2003.
[86] Daniels, H. E., 1945, ''The Statistical Theory of the Strength of Bundles of Threads .1.,'' Proc. R. Soc. London, Ser. A, **183**, pp. 405–435.
[87] Silver, F. H., Freeman, J. W., and Seehra, G. P., 2003, ''Collagen Self-Assembly and the Development of Tendon Mechanical Properties,'' J. Biomech., **36**, pp. 1529–1553.

[88] Fujii, K., Tsuji, M., and Murota, K., 1986, ''Isolation of Peripheral Nerve Collagen,'' Neurochem. Res., **11**, pp. 1439–1446.
[89] Muona, P., and Peltonen, J., 1994, ''Connective Tissue Metabolism in Diabetic Peripheral Nerves,'' Ann. Med., **26**, pp. 39–43.
[90] Stolinski, C., 1995, ''Structure and Composition of the Outer Connective Tissue Sheaths of Peripheral Nerve,'' J. Anat., **186**, pp. 123–130.
[91] Zachary, L. S., Dellon, E. S., Nicholas, E. M., and Dellon, A. L., 1993, ''The Structural Basis of Felice Fontana's Spiral Bands and Their Relationship to Nerve Injury,'' J. Reconstr Microsurg, **9**, pp. 131–138.
[92] Ushiki, T., and Ide, C., 1986, ''Three-Dimensional Architecture of the Endoneurium With Special Reference to the Collagen Fibril Arrangement in Relation to Nerve Fibers,'' Arch. Histol. Jpn., **49**, pp. 553–563.
[93] Haninec, P., 1986, ''Undulating Course of Nerve Fibres and Bands of Fontana in Peripheral Nerves of the Rat,'' Anat. Embryol. (Berl), **174**, pp. 407–411.
[94] Friede, R. L., and Bischhausen, R., 1978, ''The Organization of Endoneural Collagen in Peripheral Nerves as Revealed With the Scanning Electron Microscope,'' J. Neurol. Sci., **38**, pp. 83–88.
[95] Spilker, M. H., Asano, K., Yannas, I. V., and Spector, M., 2001, ''Contraction of Collagen-Glycosaminoglycan Matrices by Peripheral Nerve Cells In Vitro,'' Biomaterials, **22**, pp. 1085–1093.
[96] Kwan, M. K., Wall, E. J., Massie, J., and Garfin, S. R., 1992, ''Strain, Stress and Stretch of Peripheral Nerve. Rabbit Experiments In Vitro and In Vivo,'' Acta Orthop. Scand., **63**, pp. 267–272.
[97] Lambert, C. A., Soudant, E. P., Nusgens, B. V., and Lapiere, C. M., 1992, ''Pretranslational Regulation of Extracellular Matrix Macromolecules and Collagenase Expression in Fibroblasts by Mechanical Forces,'' Lab. Invest., **66**, pp. 444–451.
[98] Schild, C., and Trueb, B., 2002, ''Mechanical Stress is Required for High-Level Expression of Connective Tissue Growth Factor,'' Exp. Cell Res., **274**, pp. 83–91.
[99] Jaakkola, S., Peltonen, J., and Uitto, J. J., 1989, ''Perineurial Cells Coexpress Genes Encoding Interstitial Collagens and Basement Membrane Zone Components,'' J. Cell Biol., **108**, pp. 1157–1163.